Use of satellite imagery for automated monitoring of the shoreline retreat rate

P.G. Drakopoulos[1], E. Oikonomou[2], G. Skianis[3], S.E. Poulos[3], A.Vaiopoulos[3], K. Lazogiannis[3,4], G. Ghionis[3], A. Velegrakis[4]

[1]*Department of Optics and Optometry, T.E.I. of Athens, Athens, 12210, Greece*

[2]*Department of Civil Engineering and Surveying & Geoinformation, T.E.I. of Athens, Athens, 12210, Greece*

[3]*Department of Geology and Geoenvironment, University of Athens, 15784, Athens Greece*

[4]*Department of Marine Sciences, University of the Aegean, 81100, Mytilene, Greece*

Presenting author email: pdrak@teiath.gr

ABSTRACT

Synoptic remotely sensed data has become an essential tool for monitoring shoreline displacements while ground truthing is necessary to calibrate these images in order to detect the limits of any spatial changes. In this work we present preliminary results of an investigation regarding the reflectance properties and spectral signatures of various samples of both dry and wet sands from the beach face of Pinios river in central Greece.

Field measurements obtained with a Jaz spectrometer are compared against corresponding pixels of a few day difference WorldView-2 satellite imagery (eight spectral bands with a 2m resolution). The hyperspectral information of the field signatures is then reduced to satellite compatible normalized indices: brightness, hue, modified redness, and slope index.

The measured reflectance spectra show that different sand types have dissimilar optical properties and spectral signatures. The increased water content modifies, in a consistent manner, all indices. Once the image is properly calibrated, every pixel of the image is evaluated in terms of these indices which in turn may feed a model based on artificial neural networks (under development) with the aim to ultimately extract the shoreline position through an automated unsupervised procedure.

Keywords: Climate change, Environmental monitoring; Remote Sensing, shoreline position

1. INTRODUCTION AND THE STUDY AREA

The river deltas are regarded being highly sensitive to the effects of human imposed modifications and climate change, such as sea-level rise; their vulnerability is considered to be the result of several reasons and processes, including sediment compaction from the removal of oil, gas and water from the delta's underlying sediments, sediment trapping in reservoirs upstream, and floodplain engineering [1]. Furthermore, worldwide nearly 300 million people are living within 40 deltas, and in addition about 23% of the world's population can be found both within 100 km distance from the coast and <100 m above sea level, and with the coastal population density being about three times higher than the global average [2]. This population growth round river deltas has led to widespread conversion of natural coastal landscapes into agriculture, aquaculture, silviculture, as well as industrial and residential uses [3]. Recent studies support the above indications: in the past decade 85% from 33 indicative deltas experienced severe flooding, resulting in the temporary submergence of 260,000 km^2 [1], and satellite image analysis from fourteen of the world's major deltas indicated a total wetland loss of 15,845 km^2 over the past 14 years [4].

In particular, one of the top longest coastlines among Europe can be found in Greece with a total of approximately 16,200km and the largest urban centers are located in the coastal zone [5]. When considering economic activities, about 80% of industry, 90% of tourism and recreation, 35% of agriculture (usually of high productivity), fisheries and aquaculture, and the largest part of infrastructures (ports, airports, roads, electricity and telecommunications network etc) are located in the coastal zone [6].

Taking into account the importance of the above figures, the study area of the present work is Pinios river, having one of the most important deltas of Greece and located in Thessaly, within the central mainland section (Figure 1). The Pinios length is 216km classified as eco-region 6 for both rivers - lakes and transitional - coastal waters. Pinios river Basin lies in an area of intense agricultural activity, while food transformation and metal production industries are the most prominent [7]. The aquatic environment is affected by water level and flow regulations for flood protection, drainage channels and the coastal tourist infrastructure, with extreme hydrologic events, such as floods and droughts, being quite common in the Pinios catchment.

The Pinios River delta has a cuspate shape exposed to moderate wave activity (mean wave heights of ~1 m); the highest (although rare) offshore waves approach from the South-East and, due to long fetches, they can locally exceed 4 m in height [8]. The deltaic coast is characterized by sandy beaches with low sand dunes, consisting (mostly) of medium – sized sand abundant in quartz and feldspars. Recent observations (Thalis-DAPHNE research project) along the deltaic coast revealed seasonal changes in the shoreline position in the order of a few meters, with the exception at its mouth, where its southern part retreated by more than 10 m following a South-Eastern storm in January 2012. Therefore, monitoring the shoreline retreat rate within the vulnerable Pinios delta study area is of high environmental and economic importance and is essential for coastal management and land-use planning.
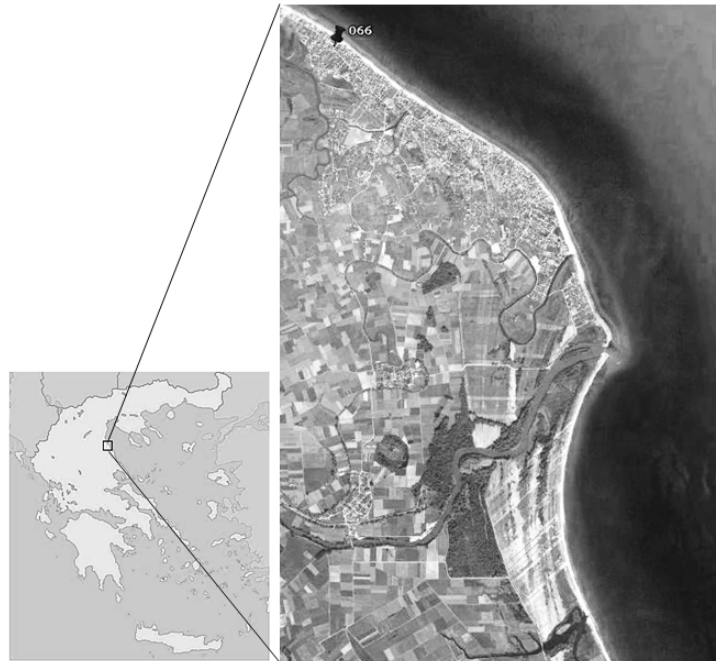

Figure1: Map of the study area and sampling site (image source: Google Earth).

In order to determine shoreline position and its retreat rate, the present work combines, on one hand, in-situ reflectance measurements and building local database of spectral signatures for the differentiation between the wet part of the lower beach face (swash zone) and its dry upper part; one the other hand, remote sensing represents a powerful tool into gaining information on the morphological beach characteristics (e.g. shoreline length/position, beach width and area) and, thus, contributing into a better understanding of the medium-term beach zone dynamics by using high resolution data from currently operational sensors, such as the WorldView-2. The potential combination and correlation between in situ reflectance measurements and satellite data analysis remains a highly promising procedure for improving the shoreline determination and the classification of the beach sediment nature. The scope of this work is to develop a cost-effective and reliable tool into identifying the shoreline position with high accuracy by calibrating satellite data through ground truthing on both the wet lower shoreface and the adjacent dry (beyond the wave reach) part of the upper beach face. The initial experiments presented here took place within the vulnerable Pinios delta and coastal zone. The ultimate aim is to further implement the results into coastal zone management as a rapid and cost-effective assessment of shoreline retreat induced by changes in mean sea level and storm surges, and in order to identify hot-spots of beach erosion.

2. FIELD REFLECTANCE MATERIALS AND METHODS

For the development of the procedure, reflectance measurements were initially performed in the laboratory. For this reason an HR4000 spectrometer, a fiber optic diffuse reflectance probe and tungsten-halogen light source at 3100 K (Ocean Optics) were employed. Reference reflectance was provided by a spectralon plate. For the field measurements, the various radiances were probed under daylight conditions through a 6º FOV Gershun tube attached via an optical fiber to a Jaz (Ocean Optics) spectrometer.

The wavelength dependent reflectance measured is defined as:

$$R(\lambda) = R_g \frac{L_{\text{sand}}(\lambda) - L_{\text{dark}}(\lambda)}{L_{\text{spec}}(\lambda) - L_{\text{dark}}(\lambda)}$$

Where $L_{sand}(\lambda)$ is the radiance from the sand sample, $L_{spec}(\lambda)$ the radiance from the spectralon plate and R_g the known reflectance of the plate. The measurements were performed with a 45° monitoring angle and with the illuminant coming from the same direction, thus avoiding possible specular components.

For classification purposes, the following indices were estimated [9,10]:

$$BI = \left[\frac{CH5^2 + CH3^2 + CH2^2}{3} \right]^{1/2} , \ HI = \frac{(2CH5 - CH3 - CH2)}{(CH3 - CH2)} , \ MRI = \frac{CH7^2}{CH2 \times CH3^3}$$

where BI is the brightness index, indicative of the average reflectance magnitude, HI is the hue index related to the dominant colour of the sample and MRI is a modified version of the redness index. The red channel is substituted by a near infrared because water appears "black" in this wavelength. We have also introduced a simple slope index: $SI=(R-B)$. The slope index is proportional to the finite element first derivative (slope from red to blue) and it is closely tied to the water content of the sample. The indices were evaluated at the center of the corresponding band of the WorldView-2 sensor (CH2 Blue=479 nm, CH3 Green=548nm, CH5 Red=659 nm, CH7 Near-IR1 =825nm) using the appropriate boxcar bandwidth.

The laboratory measurements were carried on samples from 11 beaches all around Greece. The samples were initially dry and gradually their moisture content increased whilst the reflectance was being monitored. Pinios beach in situ reflectance spectra were also collected at station 66, located 5 km north of river's outfall. In addition, beach sediment samples were analyzed granulometrically by dry-sieving (for material coarser than 0.0625 mm) and characterized according to Folk's (1980) nomenclature [11].

3. FIELD REFLECTANCE SPECTRAL RESULTS

The measured reflectance spectra showed that different kinds of sand have dissimilar optical properties and spectral signatures, as expected. Whitish sands have high reflectance (~70% in the visible part of the spectrum), whereas dark grey sands have low reflectance(~20%), with an overall ascending slope of the spectrum towards longer wavelengths (Figure 2). Colored sand samples generally have spectral curvatures associated to the dominant color. Grain size seems to contribute to the overall albedo, which increases with decreasing grain size.
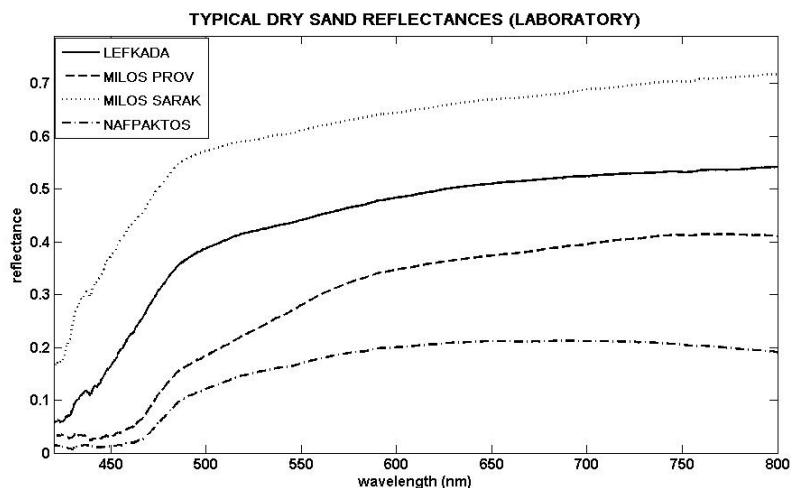

Figure 2: Reflectance spectra of different sand types as measured in the laboratory.

Experiments including dry and wet samples showed that increased wetness lowers, proportionally, the albedo of the samples across the whole spectrum (Figure 3a). Field measurements of the spectral reflectance from wet and dry sediments of the foreshore zone along the deltaic coast of Pinios river produced similar results.

Two spectral indices were found to be highly efficient in differentiating between wet and dry spectra: dry samples have high Brightness Index (average reflectance magnitude) and Slope Index, whereas increased water content in the samples results in proportionally lower Brightness Index and Slope Index (Figure 3b, 4b). Moreover, the presence of water shifts the dominant colour (Figure 3c, 4c) and the modified redness index. Therefore, depending on the water content, two separate classes of signatures exist in the four dimensional space of *BI, SI, HI* and *MRI* and can be used in order to classify beach sand samples as dry or wet accordingly. Evaluation of a similar set of classification indices proposed by Ouillion et al. [12], though for dry samples only which did not exhibit as high sensitivity for different moisture contents.
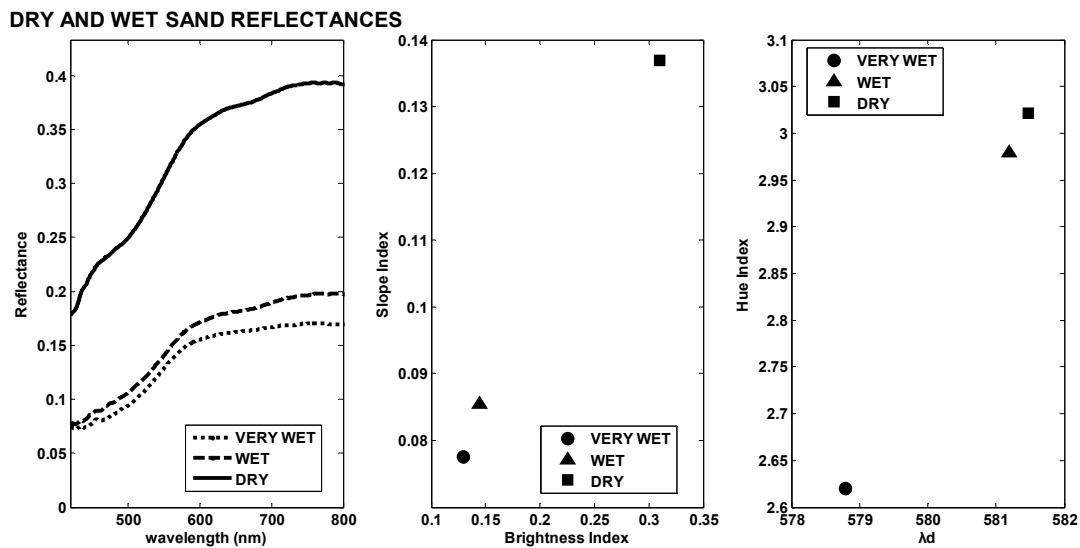

DRY AND WET SAND REFLECTANCES

Figure 3: (a) Sand reflectance spectra in the visible for variable moisture content. (b) Variation of slope index and brightness index with moisture content. (c) Variation of hue index with water content – here ploted as a function of the dominant colour. The sample is from the Glyfada beach (Near Athens).

4. SATELLITE MATERIALS AND METHODS

For the scope of the present study, a satellite image has been purchased from WorldView-2 sensor over the study area of Pinios delta acquired on June 27, 2013 at 09:35:16 UT, whereas the in situ reflectance measurements were taken a few days prior to the satellite passage. The WorldView-2 high resolution commercial imaging satellite was launched on October 8, 2009 and declared fully operational on January 4, 2010. The satellite is in a nearly circular, Sun-synchronous orbit with a period of 100.2 minutes and an approximate altitude of 770km acquiring 11-bit data in one panchromatic band (450-800nm) at 0.5m (resampled from 0.46m) spatial resolution and eight multispectral channels at 2m spatial accuracy (resampled from 1.84m), namely Coastal (400-450nm), Blue (450-510nm), Green (510-580nm), Yellow (585-625nm), Red (630-690nm), Red Edge (705-745nm), Near-IR1 (770-895nm), and Near-IR2 (860-1040nm).

In order to perform radiometric/spectral analysis onto satellite data, they must be first converted to spectral radiance and then to either a minimum or ToA (Top of Atmosphere) reflectance [13]. Going from the initial Digital Numbers (DN) to ToA reflectance is a two-step process with firstly converting the DNs into ToA radiance values and then into reflectance values [14]. According to Globe (2009, [15]) WorldView-2 products are delivered to the customer as radiometrically corrected image pixels. The values of these pixels are calculated as a function of the amount of the spectral radiance entering the telescope aperture and the instrument conversion of that radiation into a digital signal. Therefore, image pixel data are unique to WorldView-2 and should not be directly compared to imagery from other sensors in a radiometric/spectral sense. Instead, image pixels should be converted to ToA spectral radiance at a minimum. The conversion from radiometrically

corrected image pixels to spectral radiance uses the following general equation for each band of a WorldView-2 product [13]:

$$L_{\lambda(pixel,band)} = \frac{K_{band}\, q_{pixel,band}}{\Delta\lambda_{band}}$$

Where, $L_{\lambda(pixel,band)}$ are the ToA spectral radiance values in [W m^{-2} sr^{-1} nm^{-1}], K_{band} is the absolute radiometric calibration factor for a given band [W m^{-2} sr^{-1} count^{-1}], $q_{pixel,band}$ are the given radiometrically corrected image pixels [counts], and $\Delta\lambda_{band}$ is the effective bandwidth [nm] for a given band.

Both K_{band} and $\Delta\lambda_{band}$ can be found in the image metadata files (*.IDM) attached with the WorldView-2 product named as (absCalFactor) and (effectiveBandwidth), respectively. The ToA spectral radiance values can then be converted into ToA reflectance

$$\rho_{\lambda(pixel,band)} = \frac{L_{\lambda(pixel,band)}\, d_{es}^{\,2}\,\pi}{E_{sun,\,\lambda(band)}\,\cos(\theta_s)}$$

Where, $\rho_{\lambda(pixel,band)}$ are the ToA reflectance values, $L_{\lambda(pixel,band)}$ are the ToA spectral radiance values in [W m^{-2} sr^{-1} nm^{-1}], d_{es} is the Earth-Sun distance in Astronomical Units [AU], $E_{sun,\lambda(band)}$ is the WorldView-2 Band-Averaged Solar Spectral Irradiance [13] and θ_s is the average solar Zenith angle.

In order to finally convert the ToA reflectance values into surface reflectance, there exist several ways, either by using a non-linear quadratic relationship [16] or by implementing a computationally more intensive transformation available by specialized remote sensing software, such as ENVI and via its FLAASH (Fast Line-of-sight Atmospheric Analysis of Spectral Hypercubes) atmospheric correction method, which incorporates the MOTRAN (MODerate resolution TRANsmission) model and offers several options, including water and aerosol correction and atmospheric geographically dependent model schemes etc. In the present work we implemented the ENVI FLAASH procedure for a rural aerosol correction scheme but without any aerosol or water retrieval corrections.

Following the atmospheric correction, further calibration to the satellite data was achieved by applying χ^2 minimization of reflectance differences at six ground truthing stations and corresponding satellite image pixels (Figure 4). The regression showed that satellite data were overestimating field truth by an average factor (for all channels) of about 1.14.

Figure 4: Ground truthing Stations

5. COMBINED RESULTS AND DISCUSSION

In order to study the spatial behavior through the transition zone of the indices introduced above, pixels along a transect going from sea to the backshore were evaluated at station 66 (see figure 5, station also appears in Figures 1 & 4). At this location in situ reflectance measurements were taken on both the wet lower shoreface and the adjacent dry part (i.e. beyond the wave reach) of the upper beach face.

Figure 5. The across shore transect at station 66 .

In Figure 6 the field measurements are compared to the reflectance values at same location retrieved from WorldView-2, after applying the ENVI FLAASH atmospheric corrections and field calibration schemes. Figure 7 presents the reflectance profile of a cross-coast transect at station 66. The distinction between wet and dry shoreface is characterized by a reflectance increase of 0.10-0.15 (going shoreward) at the Green (510-580nm) wavelength and above. Nevertheless, at the shorter Coastal blue and Blue wavelengths (400-510nm), the distinction between wet and dry shoreface is characterized by a more restricted reflectance increase of 0.05 (going shoreward).
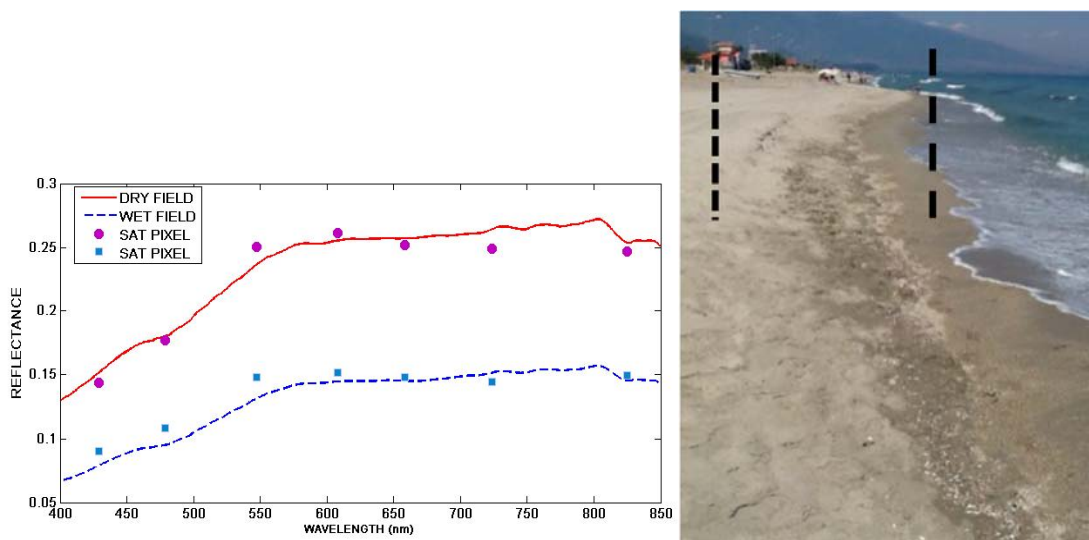

Figure 6. (a) Spectral profile of the reflectance field measurements at station 66 (for both dry and wet shoreface) compared with equivalent (nearest pixel) reflectance values at same locations retrieved from WorldView-2, after ENVI FLAASH atmospheric corrections and field calibration. (b) Field site of dry and wet sand signatures.
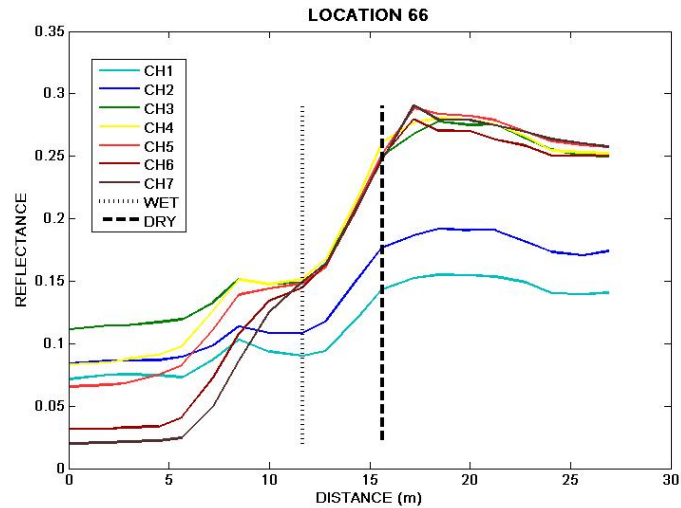
Figure 7. The reflectance profile of WorldView-2 data for a cross-coast transect at station 66 and for the seven satellite multi-spectral channels, namely Coastal Blue, Blue, Green, Yellow, Red, Red Edge and Near-IR1.

The evaluation of the indices (Figure 8) clearly shows that within the transition zone from wet to dry sand, there exists a continuous increase of the slope index, brightness index and hue index. The MRI (Modified Redness Index), which increases as the bottom depth drops, abruptly starts a reduction trend at the location of wet sand up to the point where the dry shore face begins. Therefore, the first and second spatial derivatives of this index set the limits of the transition zones.
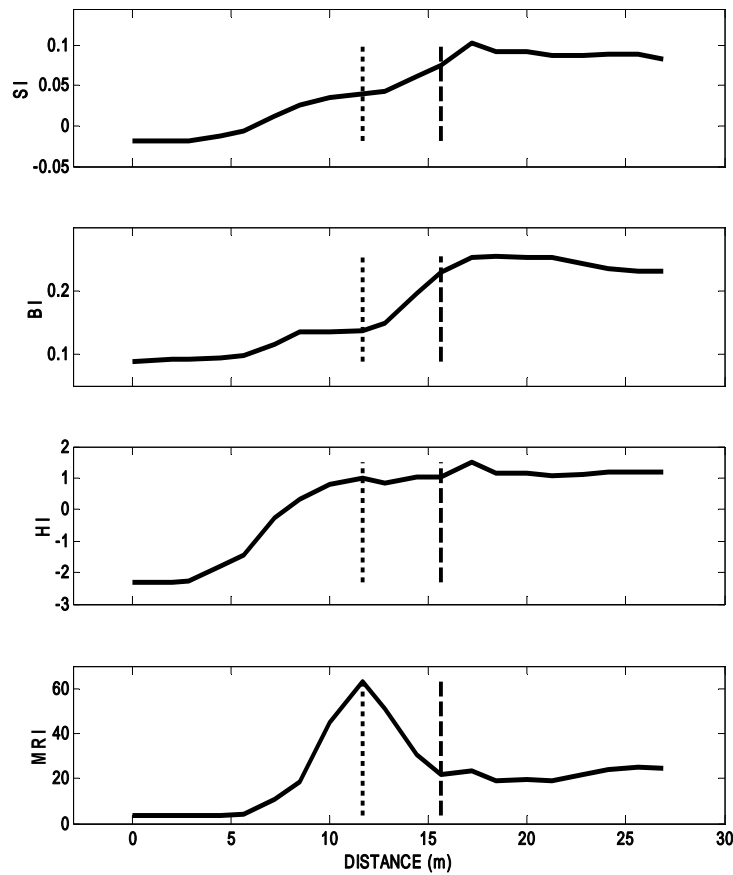

Figure 8: Evolution of various indices from sea to shore at location 66, namely (a) SI=Slope Index, (b) BI=Brightness Index, (c) HI=Hue Index and (d) MRI=Modified version of the Redness Index. The two vertical lines indicate the location where wet sand starts and ends, respectively, according to the field observations

A better feeling of the MRI significance can be obtained if all the pixels of the map section are evaluated in terms of this index (Figure 9). Width of two consecutive pixels defines the shoreline position while by applying a simple Canny edge detection function on MRI, the shoreline is revealed with one pixel (2m) resolution.

Figure 9: (a) Map of Modified Redness Index. (b) After Canny edge function is applied (Station 66)

Similar overall trends of all the indices have been also observed at another transect, at station 54 (Figure 4) south of the river mouth. This could be an indication for a broad applicability of the methodology followed.

6. CONCLUSIONS

The work here presents preliminary findings of comparing in situ reflectance measurements with co-located satellite data from the multi-spectral WorldView-2 sensor collected near the Pinios river delta, in central Greece, a both environmentally vulnerable and highly touristic region. Future work shall include the above implementation at several locations, where in situ measurements may exist, as well as expanding the methodology possibly onto other sites and high resolution multi-spectral satellite sensors. Use of satellite fusion products (spectral channels merged with high resolution panchromatic) could improve substantially the accuracy of the shoreline extraction.

Ultimately, a neural computational algorithm should be built for automatic coastal changes monitoring. Inputs will include image layers evaluated in terms of the above mentioned indices and ground truthing (training dataset) for aiding the supervised model learning procedure. The output will simply provide shoreline position with minimal human interaction.

REFERENCES

[1] J.P.M. Syvitski, A. J. Kettner, I. Overeem, E. W. H. Hutton, M. T. Hannon, G.R. Brakenridge, J. Day, C. Vorosmarty, Y. Saito, L. Giosan and R. J. Nicholls. Sinking deltas due to human activities, Nature Geoscience 2, (2009), 681 – 686.
[2] IPCC (Intergovernmental Panel on Climate Change), Chapter 6: Coastal systems and low-lying areasEds. (2007), Cambridge: Cambridge University Press.
[3] Valiela, Global Coastal Change, (2006) Oxford: Blackwell Publishing.
[4] J.M. Coleman, J.M., O.K. Huh, D.H. Braud, Jr. and H.H. Roberts, Major World Delta Variability and Wetland Loss. Gulf Coast Association of Geological Societies (GCAGS) Transactions, 55, (2005),102-131.
[5] B. Zanou, A. Kontogianni and M. Skourtos. A classification approach of cost effective management measures for the improvement of watershed quality. Ocean & Coastal Management, 46(1112), (2003), 957-983.

[6] A. Kontogianni, C Tourkolias, M. Skourtos and Papanikolaou, Linking Sea Level Rise Damage and Vulnerability Assessment: The Case of Greece. International Perspectives on Global Environmental Change, (2012), pp 375-398.

[7] Lazarou and Souflias., PINIOS PILOT RIVER BASIN – GREECE. EC Integrated Testing in Pilot River Basin proposals (2002).

[8] T. Soukissian, M. Hatzinaki, G. Korres, A. Papadopoulos, G. Kallos, E. Anadranistakis, "Wind and Wave Atlas of the Hellenic Seas", Hellenic Centre for Marine Research Publ., (2007), 300 pp., ISBN-987 960 86651 9-4.

[9] R. Mathieu, M. Pouget, B. Cervelle, R. Escadafal, Relationships between Satellite-Based Radiometric Indices Simulated Using Laboratory Reflectance Data and Typic Soil Color of an Arid Environment, Remote Sens. Environ., 66, (1998), 17-28.

[10] S.S. Ray, J.P. Singh, G. Das, S. Panigrahy, Use of High Resolution Remote Sensing Data for Generating Site-specific Soil Mangement Plan, in ISPRS Archives Vol XXXV (B7), (2004)132-137.

[11] R.L. Folk, The petrology of sedimentary rocks: Austin, Tex., (1974) Hemphill Publishing Co.

[12] S. Ouillion, Y. Lucs, J. Gaggelli, Hyperspectral Detection of Sand, Proceedings, 7th International Conference on Remote Sensing for Marine and Coastal Environments, Miami Florida (2002)

[13] T. Updike, and C. Comp, Radiometric Use of Worldview-2 Imagery. Nov. 1st ,(2010).

[14] Observation, T. Y. C. f. E., Converting Digital Numbers to Top of Atmosphere (Toa) Reflectance, (2010) http://www.yale.edu/ceo

[15] D. Globe, Digitalglobe Core Imagery Products Guide, (2009).

[16] D. Hadjimitsis, C. Clayton, A. Retalis, The use of selected pseudo-invariant targets for the application of atmospheric correction in multi-temporal studies using satellite remotely sensed imagery. International Journal of Applied Earth Observation and Geoinformation vol 11, (2009), 192-200.